THE ASTROPHYSICAL JOURNAL, 400:L1–L4, 1992 November 20

DEEP *HUBBLE SPACE TELESCOPE* IMAGING OF A COMPACT RADIO GALAXY AT $z = 2.390$[1]

ROGIER WINDHORST[2,3] AND DOUGLAS F. MATHIS[2]
Department of Physics and Astronomy, Arizona State University, Tempe, AZ 85287-1504

AND

WILLIAM C. KEEL
Department of Physics and Astronomy, University of Alabama, P.O. Box 870324, Tuscaloosa, AL 35487
Received 1992 June 22; accepted 1992 September 1

ABSTRACT

We present deep 4 hr *HST*/WFC images in V and I of the LBDS radio galaxy 53W002, a weak and compact narrow-line galaxy recently discovered at $z = 2.390$. After deconvolution, the resolution is 0.″2 FWHM. Its I-band structure is quite compact with 30% ± 10% of its flux in the central $\lesssim 1$ kpc, presumably from its AGN. This is surrounded by a clearly extended and rather symmetric envelope with effective radius $\sim 1.''1$ (4–15 kpc for $H_0 = 50$–100, $q_0 = 0$–0.5). In V, 53W002 is somewhat elongated at the same sky PA as its Lyα cloud and its VLA radio axis.

We compare 52W002's rest-frame UV profile to a properly rescaled image of a nearby early-type galaxy. The much younger starburst in 53W002 has 10–20 times higher central UV surface brightness, but otherwise an $r^{1/4}$-like light profile consistent with that of nearby luminous early-type galaxies. The available data are consistent with 53W002 being a genuinely young galaxy that only started forming stars $\lesssim 0.5$ Gyr before $z = 2.390$, but has nonetheless (just) managed to develop a rather regular light profile at $z = 2.390$, and suggest that the *dynamical collapse* of this galaxy started at about the same time as *its first major burst of star formation*. For this galaxy, both ~ 0.5 Gyr time scales are consistent with $z_{\rm form} = 2.7$–4.2 (for $H_0 = 50$–100, $q_0 = 0$–0.5).

Subject headings: galaxies: evolution — galaxies: formation — galaxies: photometry

1. INTRODUCTION

To understand galaxy formation, it would be of tremendous interest to have a clear view *at kiloparsec scales* of a galaxy that is already dynamically evolved at early cosmic epochs. This could constrain the relation between dynamics and stellar populations soon after the initial galaxy collapse. In this *Letter*, we address this issue through the first results of a deep *HST*/WFC imaging project on weak and distant radio galaxies, intended to trace their evolution in both morphology and stellar population. We concentrate on weak radio galaxies, because their optical properties are generally not dominated by an AGN, thus allowing selection of high-redshift galaxies that may give us a good view of their stellar population.

This *Letter* concentrates on the nature of the highest redshift radio galaxy—53W002—thus far found in the Leiden-Berkeley Deep Survey (LBDS; Windhorst, van Heerde, & Katgert 1984b). This radio source turned out to be a young compact galaxy ($V_{\rm tot} \simeq 22.8$ mag) with *narrow* emission lines at $z = 2.390$ and age of its starburst ~ 0.3 Gyr (as determined from ground-based spectrophotometry; Windhorst et al. 1991, hereafter W91). Our best ground-based *continuum* images show at best marginal alignment with the radio source axis, which itself is aligned with the much larger Lyα cloud (W91). Jet-induced star formation or nonthermal radiation scattered in a cone are the dominating radiation processes in the ultraluminous high-redshift 3CR and 1Jy radio galaxies (Chambers, Miley, & van Breugel 1990; McCarthy et al. 1991). It is not clear that these processes are universal, so they need to be checked for ~ 100 times weaker radio galaxies, like the ones in our LBDS sample.

2. *HST* OBSERVATIONS AND PROCESSING

2.1. *WFC Observations*

Deep (12 × 20 minute) *HST* exposures were taken in 1991 (SMS 298–299) with WFC in both the F555W ("V") and F785LP ("I") filters. We placed all targets in the center of chip WF1 since it is relatively clean, and it has the highest QE at the wavelengths of interest (Lauer 1989, hereafter L89; Griffiths 1990). Details of the observations and processing are given by Windhorst et al. (1992, hereafter W92).

Since the point-spread function ("PSF") of the *HST*/WFC combination varies strongly across the WFC field-of-view ("FOV"), a bright but nonsaturated PSF star must be available *close* to the objects to be deconvolved to assure optimal dynamic range. The $V = 19.8$ mag LBDS radio galaxy 53W044 discussed by Keel & Windhorst (1992, hereafter KW92) is 5.″5 (55 WFC pixels) away from a $V = 18.5$ mag object, whose rather red ground-based U^+J^+FN colors (Windhorst, Kron, & Koo 1984a; Kron, Koo, & Windhorst 1985) suggested a Galactic star. This was confirmed by a recent MMT spectrum, and the typical high spatial frequencies in its *HST* image. This is our best available PSF star, which we used for all our radio galaxies in the center of WF1. We also decon-

[1] Based on observations with the NASA/ESA *Hubble Space Telescope*, obtained at the Space Telescope Science Institute, which is operated by the Association of Universities for Research in Astronomy, Inc., under NASA contract NAS5-26555.

[2] Optical observations obtained in part at the Multiple Mirror Telescope Observatory, a joint facility of the University of Arizona and the Smithsonian Institution.

[3] Alfred P. Sloan Research Fellow.

volved objects with star D about 200 pixels away, for which W91 noted a faint companion 3".1 north. This turns out to be a red compact galaxy in the *HST* images with ~3% of the flux of the star. Its contamination of our alternate PSF star D did not visibly diverge this deconvolution but limits its dynamic range to ~15 dB. We found no significant differences between deconvolutions with the two different PSF stars (thus confirming the time stability of the PSF within the low dynamic range required).

2.2. *Data Processing*

A first pass through the calibration was done with the standard STScI pipeline, details of which can be found in L89. This included the following steps ([1]–[3]):

1. Correct the A/D and even/odd column problems, which add ~0.25 DN^2 to the sky variance.

2. Subtract the best available bias, dark, and preflash frames. The sky level is everywhere $\gtrsim 7$ DN in the individual exposures, so that deferred charge is not a problem.

3. Flat-field against the best available destreaked Earth flats. The signal-to-noise on the sky in the final stack is about 2%, but large-scale flat-field variations exist in WF1 of order 4%–7%. This is not objectionable since the sky level in our data is so low. The sky noise is 0.7–0.8 DN (rms) in the *average* stack after cosmic-ray ("CR") rejection (see below).

Next, we carried out the following steps:

4. Check if all *HST* orbits were pointed at the same (α, δ). The WFC images turned out to be registered well within a pixel, since the central peaks of bright stars fall consistently on the *same* pixel location in successive exposures (the rms over their peak DN was $\lesssim 2$ times larger than expected from Poissonian statistics, consistent with an rms coarse-lock pointing jitter of $\lesssim 0''.04$). This greatly simplified the CR removal routines, since no shifts had to be applied to the undersampled WFC images, which would have increased the sky variance. The *V* and *I* stacks taken a few days apart were shifted by $(\Delta X, \Delta Y) = (-2.3, +3.2)$ pixels and could be easily coregistered to increase S/N on the continuum, and blinked to find potential bad pixels.

5. Remove the myriads of CR hits in our images, since these can be quite damaging to deconvolution results. We developed and extensively tested an algorithm that iteratively determines clipped averages for each pixel over all 12 exposures (see W92 for details). *Two*-sided 2 σ clipping is done to avoid bias in the sky level (also, some residual bad pixels or columns produce *deficit* DNs that vary between exposures). If the *measured* σ value per pixel differed from Poissonian by more than 20%, it was set to the Poissonian value. For each pixel, the code usually converged in two iterations. Its progress was monitored visually in the crucial areas of interest (object and PSF stars) to make sure every pixel indeed converged to reasonable values, even in the centers of halfway-saturated stars. At the cutoff level of 2.0 $\sigma_{\rm local}$, on average 9% of *all* pixels are rejected, so that CR's rival Poisson statistics in producing spurious peaks $\geq +2.0$ σ, consistent with the steep CR count of W92, who show that CRs (with their DN counted as objects over the *entire* exposure time) have a power-law differential magnitude count $N(m) \propto m^{+0.6}$ down to our 2 σ limit of $V \simeq 30$ mag pixel^{-1} (CRs do not have the *HST*-PSF). The lowest sky variance results from clipping at the ~1.8 σ level, and we conservatively clipped the data cube at 2.0 $\sigma_{\rm local}$.

6. Found bad pixels from (4) and the STScI data quality maps and removed these through an iterative nonlinear interpolation routine that to first order preserves local SB.

7. Measure the sky brightness. At our high ecliptic latitude (+73°) it is $V \sim 23.2$ and $I \sim 22.2 \pm 0.2$ mag arcsec^{-2}. The resulting 1 σ SB sensitivity is ~27.0 in *V* and ~25.4 mag arcsec^{-2} in *I* ($\lesssim 50\%$ of the sky variance comes from read noise, the remainder from Poisson statistics, CRs below 2 σ, and residual systematic errors on the sky, the latter due to imperfectly removed streaks in Earth flats). The 6 σ point source sensitivity (with SA) is ~25.4 in *V* and ~23.7 mag in *I*. From Hunter et al. (1992) and Holtzman et al. (1991) we derive the following instrumental constants (for 1.0 DN s^{-1}) for the center of WF1 (using flats with neutral density filter F122W): 22.87 ± 0.1 mag in F555W and 21.52 ± 0.1 mag in F785LP. Before the images could be CLEANed and photometered, we needed to subtract the *local* sky from the average image, which could be done to within ~0.1–0.2 DN. The resulting *HST V* and *I* total magnitudes are—within the errors—consistent with ground-based values (W91).

2.3. *Deconvolution of the WFC Images with σ-CLEAN*

The images were deconvolved with the "σ-CLEAN" algorithm, as described by Keel (1991) and King et al. (1991). This is a modification of the classical Högbom (1974) CLEAN adapted to the photon-limited regime. It uses the CCD equation to select the *most significant* (*not* the highest) component from the residual image in each iteration. Both simulations and experience with the King et al. (1991) WFC images show that *HST* data can be deconvolved to nearly the diffraction-limited performance, but only with limited dynamic range (15–20 dB). Virtually all structure that σ-CLEAN restores above the local noise level was found in the original image, giving some confidence in the results for real galaxies. CLEANing is typically done to a level of 3.0–3.5 σ, depending on the quality and noise uniformity of the stacked image. The exact limit is a compromise between not removing enough of the PSF wings and increasing the image noise too much by CLEANing too deeply, which amplifies spurious noise. After CLEANing has converged, the δ functions are convolved with a Gaussian of FWHM = 0".2 (to satisfy the Nyquist criterion for WFC) and the result was added back into the residual image. Because of the PSF variations across the WFC FOV, we CLEANed subimages not exceeding ~240 × 240 pixels with the closest PSF star.

2.4. *Application of a Hybrid CLEAN on Extended Objects*

In order to improve the S/N at low spatial frequencies without a noise penalty at high frequencies, we also applied the *multiresolution* CLEAN of Wakker & Schwarz (1988, hereafter WS). They smooth both image *and* PSF with a Gaussian (with FWHM ≃ the object's FWHM) to produce a *low* spatial frequency image, which is subtracted from the original image, so that the *difference* image contains primarily its *high* spatial frequencies. Both images are then deconvolved separately with their appropriate PSFs. This reduces the noise that a *single* CLEAN would introduce at high frequencies (since it overinterprets the low frequencies as point sources). To avoid negative fluxes as in the radio-astronomy WS implementation, we replaced Gaussian smoothing with a median filter (see KW92). First, a trial deconvolution is done (with the normal σ-CLEAN), and the resulting CLEANed image is median-filtered with a 10–20 pixel box size. This low-frequency image is convolved with the *actual HST* PSF (so that it represents the low frequencies as seen through *HST*), and then subtracted from the raw image stack. The remaining high-frequency image is

largely positive and then deconvolved with the usual σ-CLEAN, and the results are added back into the CLEANed low-frequency image. This procedure is valid because convolution and addition commute. We also deconvolved our images with the Lucy (1974) algorithm as implemented within STSDAS and did *not* find significantly different image structures (except that CLEAN gives sharper object cores, as expected from the performance of these algorithms at various spatial frequencies).

3. STRUCTURE OF THE DECONVOLVED WFC IMAGES

Figure 1 (Plate L1) shows the 8 hr $V+I$ stack of 53W002 after deconvolution. This broad-band continuum image reaches substantially deeper than the 3000 s 200 inch (5 m) Four-Shooter Gunn $g + r$ exposure displayed in W91. Most objects are faint, high-SB galaxies with $V \lesssim 25$ mag. A faint stellar image in the lower left of Figure 1 attests to the reliability of the deconvolutions. Our WFC images (Figs. 1 and 2 [Pl. L2]) show that 53W002 is partially resolved. Its intensity profiles (Fig. 3) may be fitted by an unresolved central source (AGN or compact core) plus an extended galaxy envelope. Fits were done to the *undeconvolved* images as well, to ensure against errors introduced by deconvolution. Under the physically plausible assumption that the galaxy surface brightness (SB) is monotonic with radius, the core contributes at most 20% in V ($\lambda_{rest} \simeq 1600$ Å) and 25% in I ($\lambda_{rest} \simeq 2600$ Å), with a secure upper limit of 37%, consistent with the ground-based spectroscopic limits to 53W002's continuum AGN contribution ($\lesssim 35\% \pm 15\%$; W91). After subtracting a $30\% \pm 10\%$ AGN component, the rest-frame (stellar) UV light corresponds to $V = 23.3$ and $I = 22.5 \pm 0.2$ mag, within the errors consistent with ground-based aperture photometry of W91. Most of the galaxy's light comes from the central 1".1 radius ($\simeq$4–15 kpc; hereafter we quote all physical parameters for the range $H_0 = 50$–100, $q_0 = 0$–0.5, unless stated otherwise).

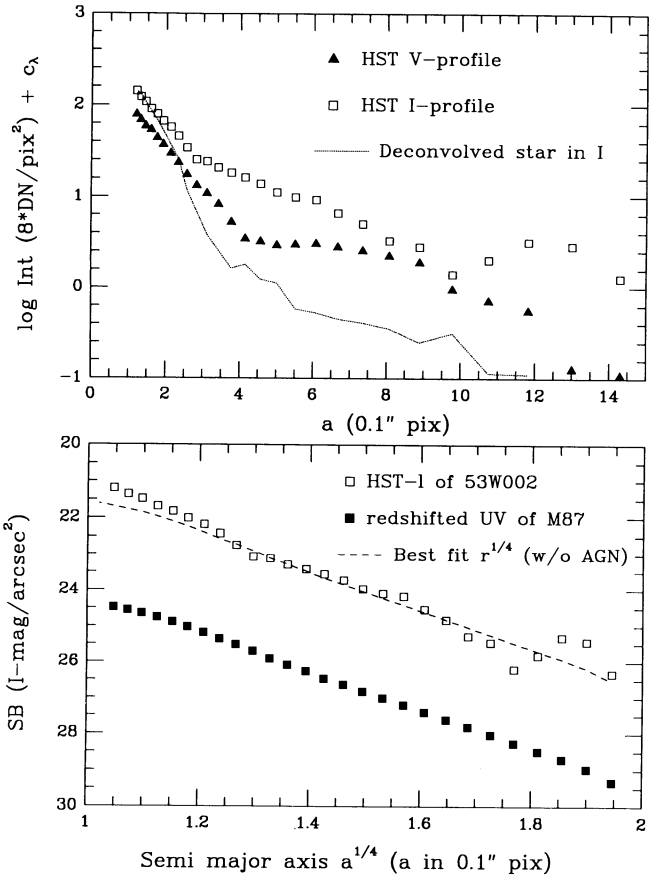

FIG. 3.—Light profiles through the deconvolved WFC images of 53W002. *Top*: Filled triangles indicate F555W ("V"), open squares F785LP ("I"). The dotted line indicates the deconvolved star (*not* the PSF) of Fig. 1 in F785LP. The galaxy 53W002 is clearly extended with respect to this star. *Bottom:* Light profiles through the deconvolved I-band image of 53W002 (*open squares*) and the properly redshifted, repixelated, and K-corrected image of M87 (*filled squares*; see also Fig. 4). Dashed line is an $r^{-1/4}$ profile that matches the outer parts of 53W002. For radii $\lesssim$0".2, 53W002 shows excess light from the central point source, that contains about 30% ± 10% of the total light.

The ground-based redshifted Lyα image of W91 clearly shows that 53W002 is extended at sky PA = 96° ± 5° (roughly *horizontal* in Fig. 1 under this *HST* orientation). The 0".7 VLA 8.4 GHz radio source of W91 is also extended in the same direction (PA = 90° ± 3°). Concentric elliptical isophote fits to the WFC images only show a marginal elongation ($e = 0.2 \pm 0.1$) of the V- and I-band *continuum* at PA $\simeq$ 105° ± 10°. Although this PA is within the errors the same as that of the redshifted Lyα and VLA 8.4 GHz images, the optical continuum has a rather small effective radius. Both the radio source and the marginally aligned WFC V-band continuum have about the same physical size ($\lesssim$0".6, or 2.4–8 kpc at $z = 2.390$). The Lyα cloud is much larger (3" × 5", or 12 × 20–40 × 67 kpc). Any continuum "alignment effect" in this *lower power* radio galaxy does thus not extend over as large a physical distance as in the *most luminous* high-redshift radio galaxies.

4. DISCUSSION AND CONCLUSIONS

Our deep *HST* images show that the weak radio galaxy 53W002 is centrally condensed, even after accounting for the 30% ± 10% contribution from its AGN. Figure 3 shows that 53W002 has a radial intensity profile that can be equally well fitted by a de Vaucouleurs profile or an exponential disk (i.e., a "generic" galaxy profile), in contrast with the much larger, clumpy ultraluminous radio galaxies observed from the ground (e.g., McCarthy et al. 1987; Chambers et al. 1990).

4.1. *Comparison of 53W002 to Nearby Early-Type Galaxies*

The radio power of 53W002 is log $P_{1.4} = 27.29$ W Hz^{-1} (for $H_0 = 100$, $q_0 = 0$), or $\sim$2.5 dex larger than the P^* value that separates FR II from FR I sources at $z = 0$ (although P^* may also evolve with cosmic epoch), and $\gtrsim$5 dex larger than the most powerful known radio spirals at $z = 0$. Hence, unless spiral or Seyfert galaxies underwent much stronger cosmological evolution as radio sources than giant ellipticals (gE's) and quasars, 53W002's radio power indicates that it likely belongs to the parent population of early-type galaxies, and thus not likely had a disk at $z = 2.390$. For this reason, we compare 53W002's light profile with that of nearby, luminous early-type galaxies with moderately powerful radio sources. Windhorst, Mathis, & Neuschaefer (1990) suggested that a high-redshift galaxy of moderate radio power like 53W002 may well have gE's as nearby counterparts, since they form a good match in radio luminosity and space density (assuming these properties undergo the usual cosmological evolution).

Figure 4 (Plate L3) shows how the *unevolved* gE elliptical galaxy M87 would appear if observed by *HST* at $z = 2.39$. For this, we used a Lowell R-band image of M87 that covers a 9'.4 × 9'.4 FOV. Using a Virgo distance of 18 Mpc, the M87 image was rebinned 25 × 25 to match the linear scale of 53W002 at $z = 2.390$ (using $H_0 = 100$, $q_0 = 0$, so that each 0".1

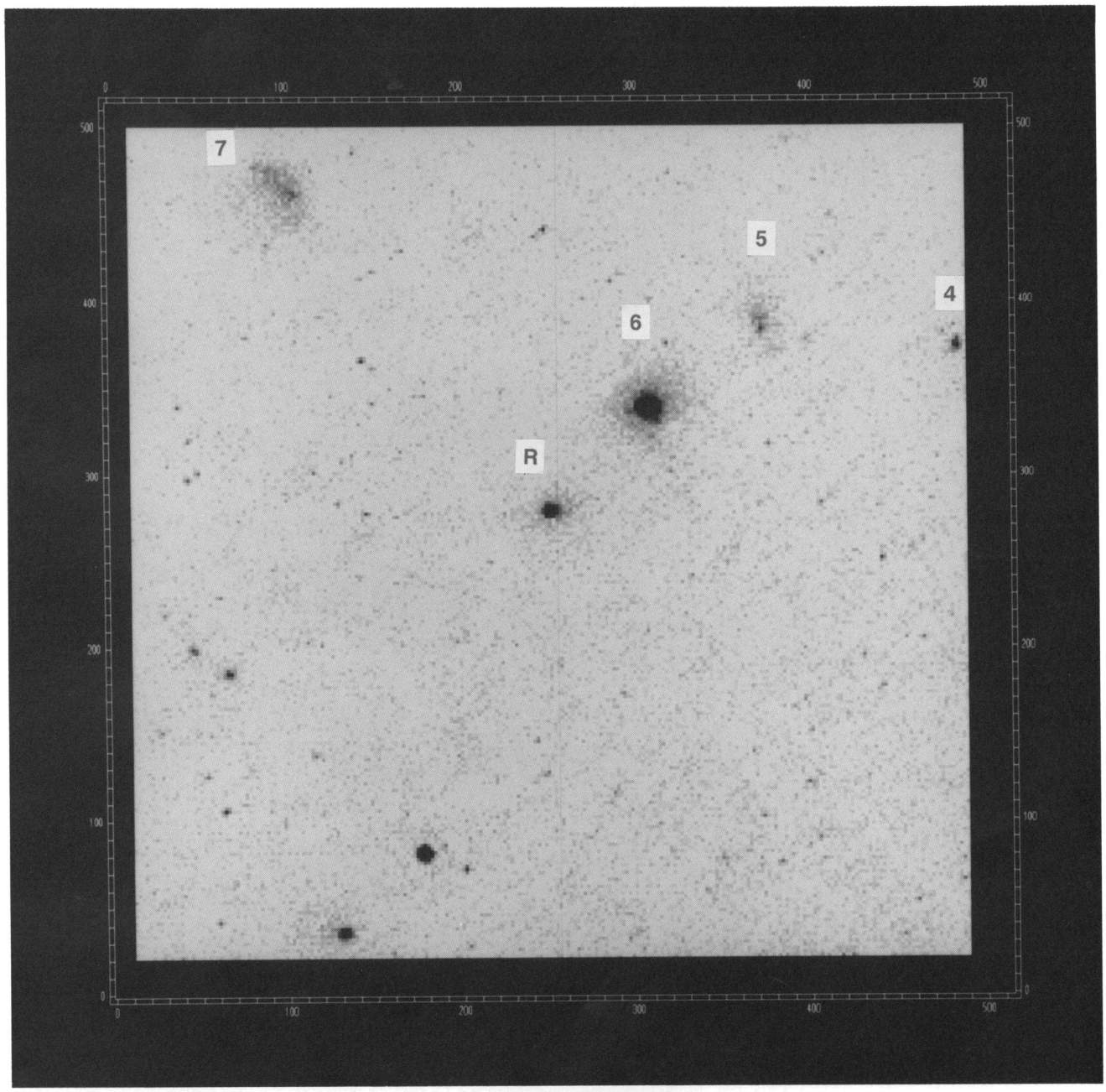

FIG. 1.—Stack of 24 × 20 minute exposures with *HST*/WFC in F555W + F785LP on 53W002 *after* deconvolution to a resolution of 0.″2 FWHM. The image has 0.″1016 pixels, and the area shown is 24.″4 on a side. The stack reaches a 1 σ SB sensitivity of $R \simeq 26.2$ mag arcsec^{-2} and has a 6 σ point source sensitivity of $R \simeq 24.6$ mag. The brighter of the two objects at the southern edge is a star, used to verify the quality of the deconvolution. The $V = 22.8$ mag radio galaxy 53W002 at $z = 2.390$ is labeled "R" and is clearly resolved compared to this star (whose peak intensity is $\sim 6\times$ higher than 53W002 in F785LP). The morphology of 53W002 is nonetheless rather compact. At this *HST* orientation, the vertical axis has sky PA $= +5°$. The redshifted UV continuum of 53W002's outer envelope is aligned with its radio and Lyα axis (both at sky PA $= 95° \pm 10°$), but only on 0.″4–0.″6 scales. Other galaxies are labeled "4, 5, 6, and 7," as in W91. The thin vertical line (along CCD rows in the middle) is a display defect in the Dicomed.

WINDHORST, MATHIS, & KEEL (see 400, L3)

PLATE L2

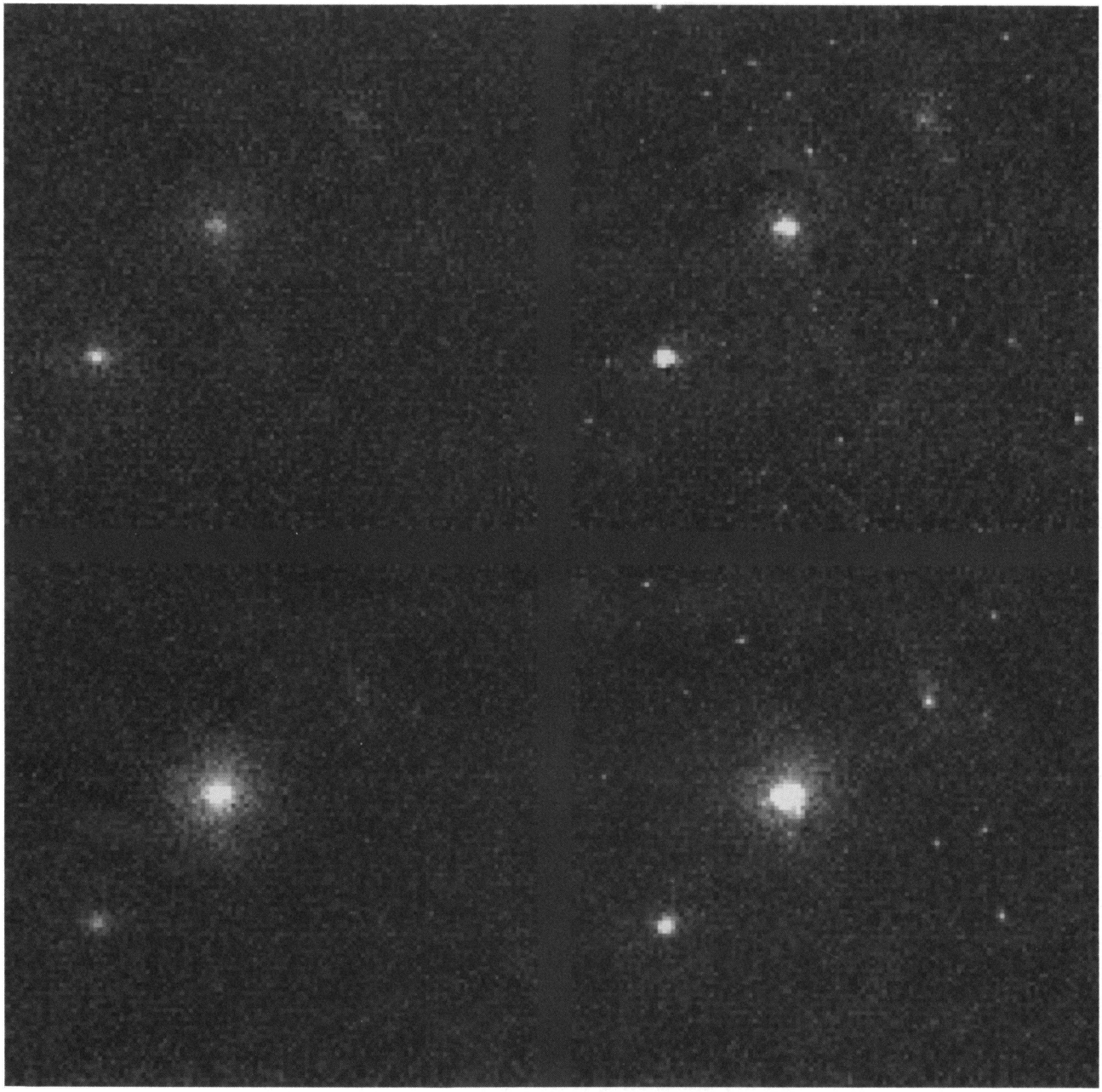

FIG. 2.—Stack of 12 × 20 minute *raw and deconvolved* WFC images of 53W002 in F555W (*top*) and F785LP (*bottom*). In each case, the aberrated image is to the left and the multiresolution σ-CLEANed version to the right. All have the *same* intensity mapping per DN. The image area shown is 12.2 arcsec^2. Orientation is as in Fig. 1. The radio galaxy 53W002 at $z = 2.390$ is the SE (*lower left*) of the three prominent objects. Note that 53W002 is rather blue in $V-I$, and object 6 is rather red (a foreground galaxy with an MMT spectrum indicating $z \gtrsim 0.52$).

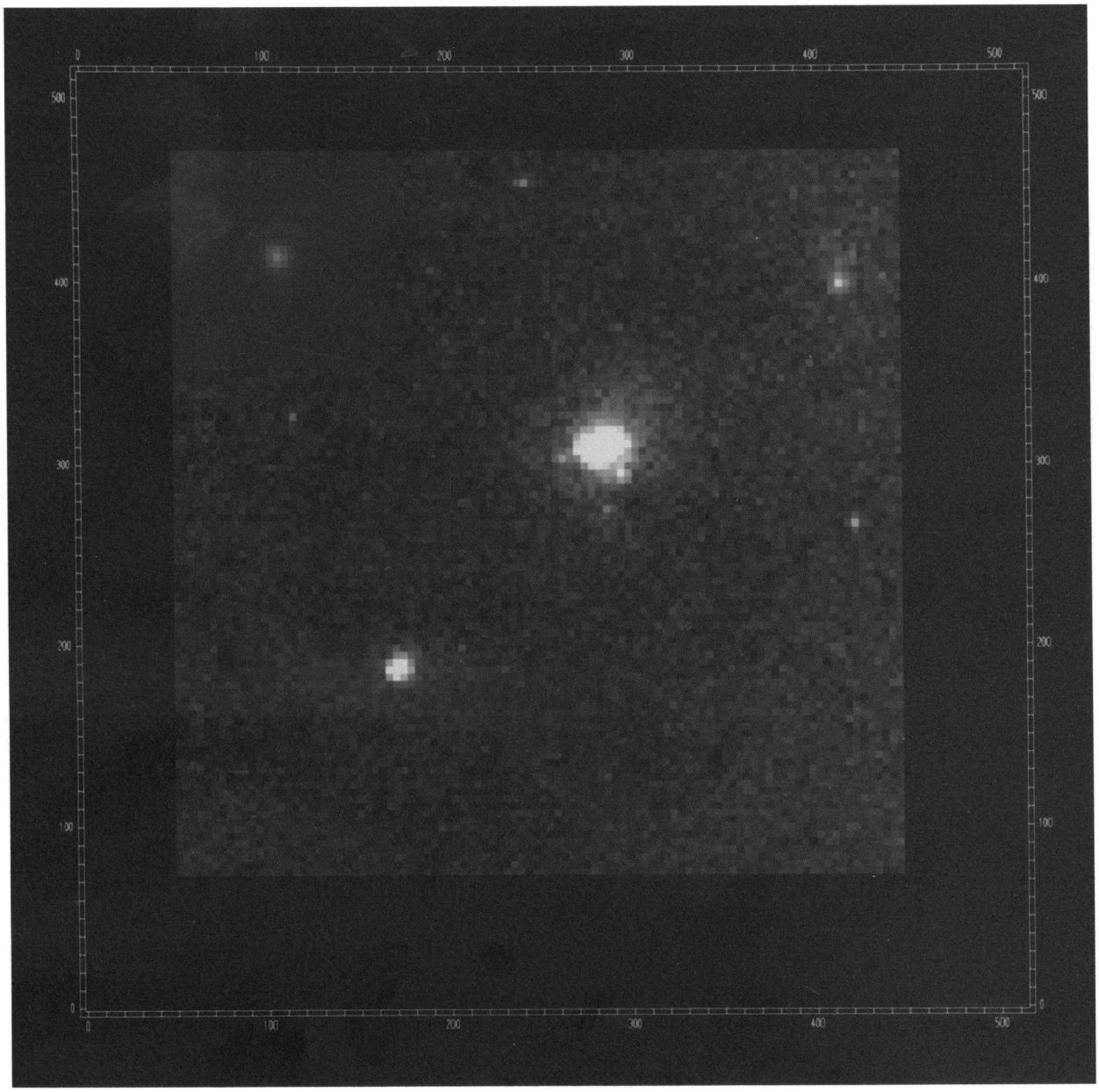

FIG. 4.—Stack of 12 × 20 minute exposures with *HST*/WFC in F785LP on 53W002 *after* deconvolution. Orientation is as in Fig. 1. The inserted panel at the upper left is a rebinned ground-based Lowell 1.1 m CCD image of M87, as it would appear at the same redshift and rest-frame passband (see text for details). Again, 53W002 is at lower left. 53W002's central SB includes a 30% ± 10% point source (in the central $\lesssim 1$ kpc pixel) and its profile is brighter (although noisier) than M87 in the rest frame UV at *all* radii. Most of 53W002's light is concentrated in a faint and nearly symmetric halo with effective radius $\sim 1\farcs1$ ($\simeq 4$–15 kpc), presumably its stellar population. Note that the linear scales of the two galaxies are similar.

pixel subtends 0.66 kpc). We used the *IUE* spectra of Keel & Windhorst (1991) and estimated the F_λ (2600 Å)/F_λ (5500 Å) flux ratio (observed I corresponds to 2600 Å at $z = 2.39$) to be ~ 0.13. This was converted to a continuum luminosity using M87's integrated RC2 photometry (the classical K-correction is thus included empirically, but *no* evolutionary correction is included, since the purpose is to see differences between high-SB galaxies with cosmic time). The expressions from Weedman (1986) were used to compute M87's *observed* intensity at $\lambda = (1 + z) \times 2600$ Å, correcting for the appropriate $\propto (1 + z)^{-4}$ bolometric SB dimming. The rebinned M87 image was scaled to the proper integrated I-magnitude and converted to WFC-like DN accounting for the difference in telescope and detector sensitivity and gain.

Figure 4 compares this M87 image and our deconvolved I image of 53W002 on the *same linear and intensity scales* (in WFC-DN). Surface photometry was performed on the rebinned M87 image after smoothing with a 0".2 FWHM Gaussian to simulate what it would look like to WFC at $z = 2.390$. For the cosmology above, M87 would have $I = 25.33$ mag, about 3 mag fainter than the stellar population in 53W002 (see also Figs. 3 [*bottom*] and 4). Figure 4 shows that a radio galaxy like 53W002 at $z = 2.390$ must have undergone a fair amount of luminosity evolution *if* its nearby counterpart is a luminous gE galaxy, since it is substantially brighter than one of the most luminous early-type galaxies seen *nearby* at the same rest-frame wavelength.

To explore the range of allowable light profiles consistent with the data, we fitted a range of de Vaucouleurs profiles (with effective half-light radius in the range 10–35 pixels) plus various nuclear point source contributions (amounting to 20%–60% of the total light) to 53W002's *aberrated* I-band image where the galaxy *envelope* has somewhat higher S/N than in V. The PA and axial ratio of the models were set to match the outer isophotes in the $V + I$ stack, where we have the best overall detection. These models were then convolved with the actual PSF, subtracted from the raw data, and their reduced χ^2 was determined. The best χ^2 fit to the I-image occurs for a point-source contribution $30\% \pm 10\%$ and an effective radius $r_e \simeq 10$–12 pixels (along the major axis), corresponding to 13–16 kpc for $H_0 = 50$ and $q_0 = 0$, and 4–5 kpc for $H_0 = 100$ and $q_0 = 0.5$, and bracketing the 8.2 kpc RC2 value for M87. Since the measured intensity slope is taken to the fourth power, a 20% flux error may well cause the 0.3 dex scale length difference between the deconvolved χ^2 models and the RC2 value, so that we cannot use the current images to constrain H_0 and q_0.

4.2. *Comparison to Models and Conclusions*

The stellar population of 53W002 is spectroscopically dominated by stars of ages 0.3 Gyr (but not likely exceeding 0.5 Gyr; W91). Let us consider this in comparison with the dynamical appearance of the galaxy. 53W002 has undergone sufficient relaxation to have a monotonic *HST* profile without bright clumps, in contrast with objects 3 and 7 (only the latter is shown in Fig. 1), for whom W91 suggested that they could be Lyα-emitting galaxies at the same redshift. At $z = 2.390$, 53W002 already shows the appropriate light profile and scale size consistent with the present-day structure of a luminous high-SB galaxy. Van Albada (1982) has modeled the collapse of protogalaxies and finds that smooth structure is achieved after a *few* crossing times (of the final galaxy), or ~ 0.5 Gyr. Also, 53W002's rather regular light profile suggests that this galaxy could *not* have undergone a major merger just before we see it. The existence of isolated luminous high-SB galaxies at early cosmic times thus suggests that at least some ellipticals may have formed without (early) mergers.

As argued from its radio power in § 4.1, 53W002 is not likely to have had a disk at $z = 2.390$. Its collapse must thus have been rather efficient (or the remaining gas would have likely formed a disk), but also *recent* given the *young age* of its stellar population. Hence, we believe that 53W002 is also *dynamically* a young galaxy which, however, is dynamically *no* younger than its stellar population. Its collapse as protogalaxy likely did not start *more* than ~ 0.5 Gyr *before* $z = 2.390$, which places its formation redshift at 2.7–4.2, i.e., after the first quasars appeared.

In conclusion, our main findings are (1) 53W002 has a well-behaved, generically galaxy-like light profile already at $z = 2.390$; and (2) this profile is consistent with a luminous early-type present-day galaxy like, e.g., M87. At least this one radio galaxy is already dynamically relaxed, hence a few crossing times old at $z = 2.390$. Within the errors, its dynamical age is consistent with that of the stellar population ($\lesssim 0.5$ Gyr; W91) so that its *dynamical collapse and its first major burst of star formation* may have started at the *same* time. Some galaxies therefore formed rather quickly and possibly as late as $z_{\rm form} \lesssim 2.7$–4. Objects like 53W002 appear to still be undergoing their *first* major epoch of global star formation at $z \simeq 2.4$ and may be showing us the later stages of a protracted epoch of galaxy formation.

We thank Ray Lucas, Bruce Gillespie, Dan Golombek, and the STScI staff for their continuous help in this project; Jonathan Gordon for help with the data processing; the Director of Lowell Observatory for 1.1 m time; Jeff Hester and Tod Lauer for helpful discussions; and the referee Hy Spinrad for useful comments. This work was supported by NASA grant GO-2405.01-87A (to both R. A. W. and W. C. K.) from STScI, which is operated by AURA, Inc., under NASA contract NAS5-26555, and by NSF grant AST 88-21016 and the Alfred P. Sloan Foundation (to R. A. W.).

REFERENCES

Chambers, K. C., Miley, G. K., & van Breugel, W. J. M. 1990, ApJ, 363, 21
Griffiths, R. G. 1990, in *HST* Telescope Wide Field and Planetary Camera Instrument Handbook, Version 2.1 (Baltimore: STScI)
Högbom, J. A. 1974, A&AS, 15, 417
Holtzman, J. A., et al. 1991, ApJ, 369, L35
Hunter, D., Faber, S., Light, R., & Shaya, E. 1992, in Final Orbital/Science Verification Report of the WF/PC IDT, ed. S. M. Faber & J. A. Westphal (Baltimore: STScI)
Keel, W. C. 1991, PASP, 103, 723
Keel, W. C., & Windhorst, R. A. 1991, ApJ, 383, 135
———. 1992, in preparation (KW92)
King, I. R., et al. 1991, AJ, 102, 1553
Kron, R. G., Koo, D. C., & Windhorst, R. A. 1985, A&A, 146, 38
Lauer, T. 1989, PASP, 101, 445 (L89)
Lucy, L. B. 1974, AJ, 79, 745
McCarthy, P. J. 1987, ApJ, 319, L39
Van Albada, T. S. 1982, MNRAS, 201, 939
Wakker, B. P., & Schwartz, U. J. 1988, A&A, 200, 312 (WS)
Weedman, D. W. 1986, in Quasar Astronomy (New York: Cambridge Univ. Press), 59
Windhorst, R. A. Kron, R. G., & Koo, D. C. 1984a, A&AS, 58, 39
Windhorst, R. A., Mathis, D. F., & Neuschaefer, L. W. 1990, in Evolution of the Universe of Galaxies (Edwin Hubble Centennial Symposium), ed. R. G. Kron (ASP Conf. Ser., 10), 389
Windhorst, R. A., van Heerde, G. M., & Katgert, P. 1984b, A&AS, 58, 1
Windhorst, R. A., et al. 1991, ApJ, 380, 362 (W91)
Windhorst, R. A., et al. 1992, in preparation (W92)